Chapter

Unshielded Magnetocardiography in Clinical Practice: Detection of Myocardial Damage in CAD Patients and in Patients Recovered from COVID-19

Illya Chaikovsky, Anatoly Kazmirchyk, Sergey Sofienko, You-Bin Liu, Ya-Feng Zhou, Xie Feng, Lin Xu and Yan-Fei Huang

Abstract

The chapter deals with magnetocardiography—a specific section of electrocardiography, which is designed to analyze the magnetic component of the electromagnetic field of the heart. Magnetocardiography is described as clinical information technology (IT), i.e., a set of methods, software, and hardware combined into a technological chain, the product of which is an automated diagnostic report. There are several examples of magnetocardiographic information technology implementation in clinical routine, aiming to register and evaluate subtle changes in the electromagnetic field of the heart for early diagnosis of the most common and dangerous heart diseases, especially coronary heart disease. It is shown that new metrics of analysis of spatial structure of 2D and 3D magnetocardiographic maps of current density distribution allow diagnosis with high accuracy of various forms of myocardial ischemia as well as myocardial damage in patients, recently recovered from COVID-19.

Keywords: magnetocardiography, coronary artery disease, non-coronarogenic diseases, myocardial damage, COVID-19, pattern recognition

1. Introduction

Effective diagnosis of heart disease remains one of the main tasks of clinical medicine due to the high prevalence and socio-economic importance of diseases such as cardiovascular diseases, which in recent decades, have become a pandemic [1]. In most European countries per 100,000 people. Population accounts for no more than 300 deaths from cardiovascular diseases. It is clear that the need to improve methods

for heart diseases detection is extremely actual. First of all, this applies to non-invasive methods that are the most accessible and safe.

Analysis of the electrical activity of the heart is still the most common, affordable, and cheapest method of objective examination of the heart. However, the sensitivity and specificity of routine electrocardiographic examination are not high enough. It is known, for example, that the resting ECG, assessed by its routine criteria, remains normal in approximately 50% of patients with chronic coronary heart disease, including during episodes of chest discomfort [2]. Improving diagnostics is possible only on the basis of innovative technologies.

The purpose of this chapter is to give an example of innovative technology introduced into practice, designed to register and evaluate subtle changes in the electromagnetic field of the heart for early diagnosis of the most common and dangerous heart diseases.

2. MCG definition and a brief insight to the magnetocardiography milestones

Magnetocardiography allows recording magnetic fields without body invasion and any risks through the skin-surface methodology. The detected fields are created by the heart's electrical activity. However, the signal is pretty weak to export the samples for storing and assessment, making the technique demanding, e.g., typical level of a magnetic field generated by heart muscle currents is between 10^{-10} and 10^{-12} Tesla, whereas the Earth's magnetic field and the urban noise levels are considerably higher (**Figure 1**).

The 1963 study by McFee and Balue records the first magnetocardiograms [3]. To obtain the game-changing magnetocardiogram human data they applied a couple of coils, containing a ferromagnetic core wrapped around with thin copper wire for

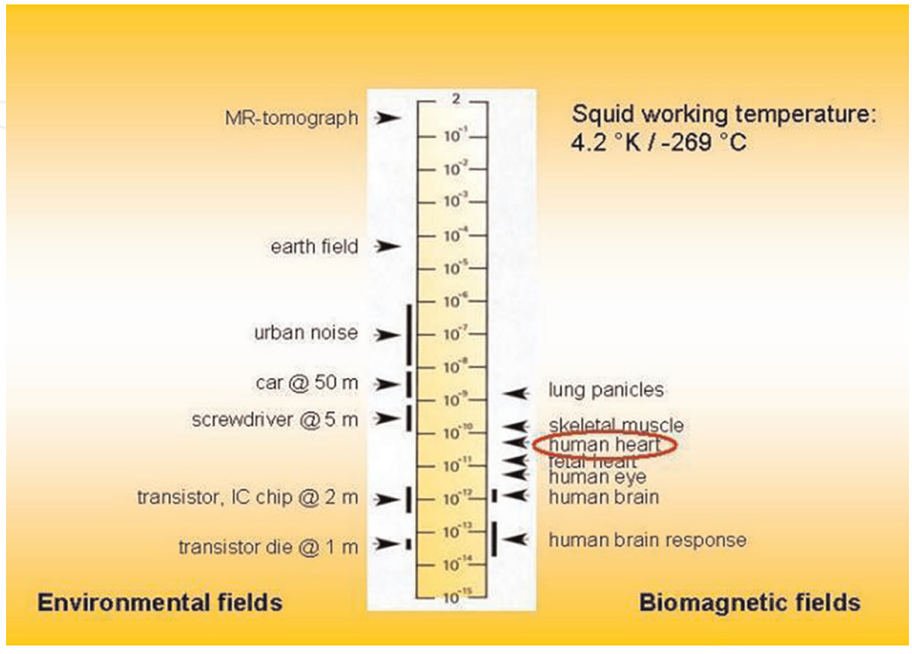

Figure 1.
Specimens of generated magnetic fields.

several million times in each, kept at room temperature. The experiments were held at a far-away country location, to avoid the urban electromagnetic hindrance. Nevertheless, the output of the detector had flaws.

The research progress for alloys in the early 70's introduced the use of superconducting magnetometers. Cohen at al. initially applied the superconducting quantum interference device (SQUID) magnetometer in a room with antimagnetic protection, to detect a magnetocardiogram with improved dimensional accuracy and better spatial-to-noise property.

These SQUID magnetometers remain the only available device to record MCGs. The MCG studies by Cohen at al. had an enormous contribution to the basics of MCG recordings methodology, but cannot be considered a clinically relevant study, even though physicians took part in a few measurements. Then, in the early 80's Germany, USA, Finland, Japan, and Italy had some preliminary clinical research studies. At that time, a sole SQUID sensor was moved step by step across the measurement layout at the area near the anterior torso. The first commercially-made multi-channel systems became available in 1988–1990 with the help of Siemens, Philips, and BTI cooperation. In fact, only properly shielded rooms could be used for those systems' operation (**Figure 2**).

Today, there are numerous MCG laboratories in countries such as the United States, Germany, China, South Korea, Italy, Finland, Great Britain, Russia, Japan, Taiwan, India, and others.

In Ukraine, research in the field of magnetocardiography was initiated by specialists of the Institute of Cybernetics. VM Glushkov NASU together with specialists of the Institute of Cardiology in 1992. These studies began with the use of a single-channel MCG system. The work of the Kyiv group was pioneering from the very beginning because it was aimed at solving the most pressing problem—the diagnosis of coronary heart disease in difficult cases, i.e., in patients with uninformative results

Figure 2.
Philips multi-scan MCG system inside a highly-shielded room.

Figure 3.
9-channel MCG-system (Cardiomox) in unshielded hospital setting.

of routine tests such as ECG and resting echocardiography [4, 5]. Also, it is extremely important that the magnetocardiographic system developed by Ukrainian scientists can work in a normal unshielded room, which made the method of magnetocardiography suitable for wide clinical application (**Figure 3**).

3. Technical means of magnetocardiography and procedure of patients examination

Measurement of ultra-weak magnetic fields that occur during the work of the human heart and are almost a million times smaller than the magnitude of the Earth's magnetic field ($\approx 10^{-4}$Tl), requires very sensitive equipment. A significant increase in the sensitivity of biomagnetic measurements was achieved with the introduction of SQUID magnetometers, which operate on the basis of the stationary Josephson effect at a temperature of liquid helium (4.2 K). Beginning in 1970, when the SQUID magnetometer was first used [6], the MCG registration procedure became available for medical research and clinical practice.

Each of the currently known MCG systems can be divided into three functional modules. The first module (measuring) contains a registration part, which consists of sensors, antenna systems, and electronics for reading sensor signals. The second module (control) includes electronic units and microprocessor control of the entire system. The third (software module) provides computer processing of signals and their display using an application package with a high level of intelligent software. Additional hardware and software for protection against magnetic interference are used in each module.

Our MCG-system CARDIOMOXMCG 9 is installed in an unshielded clinical setting and during normal daytime operation, environmental noise was relatively constant. During acquisition, power lines represent the most dominant source of high amplitude noise (**Figure 4A**).

The position of the examined object is idle on the back. The MCG detections are held inside a six-by-six rectangular nettings that create an area (4 cm^2) over the precordial area making nine prethoracic sites. The sensor is moved to the thorax as

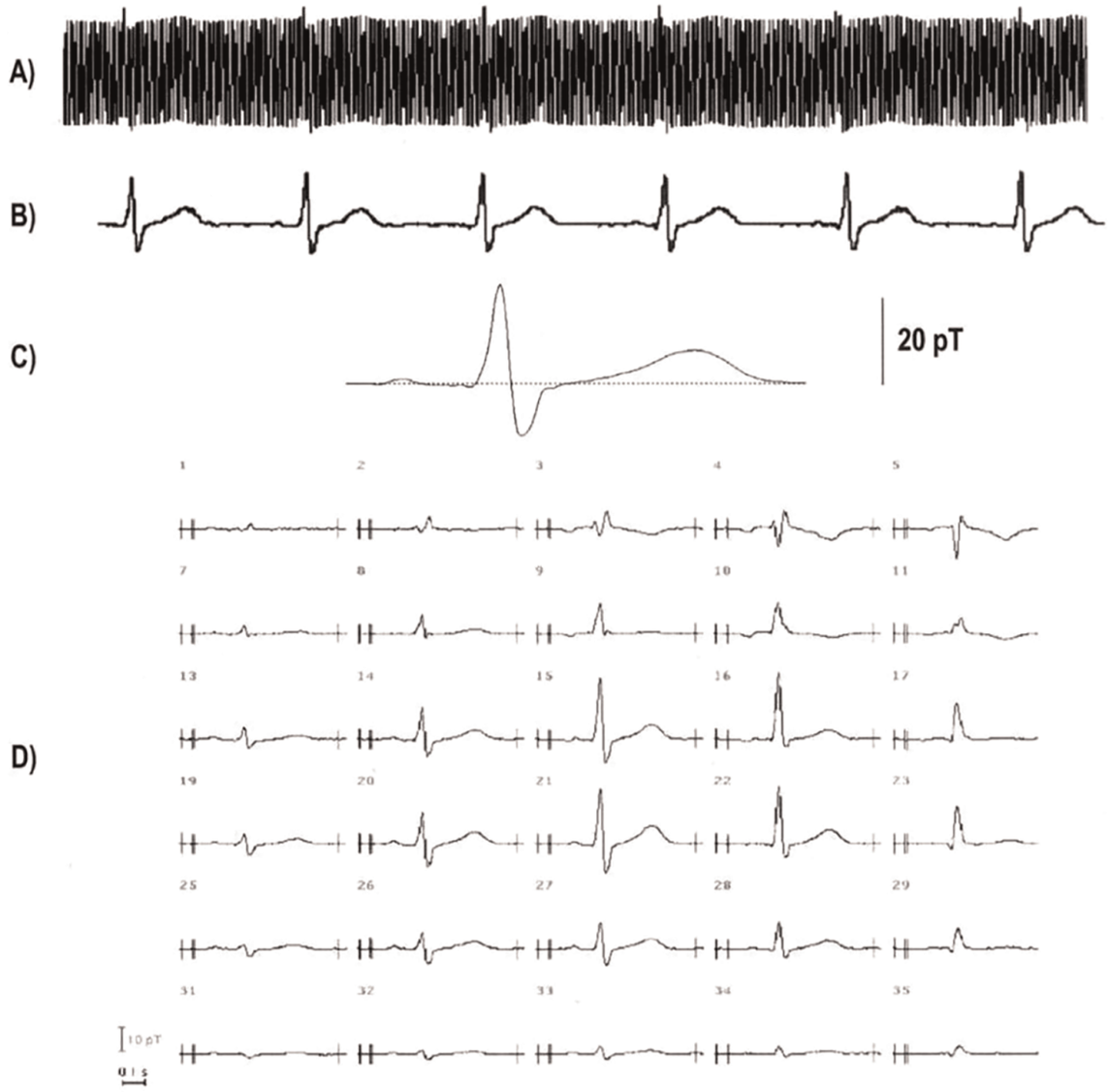

Figure 4.
Samples of the MCG signals. (A) Initial channel 21 output (power noise included), (B) Same channel: 50 Hz notch filtered data, (C) Same channel: averaged signal, DC offset corrected prior to the P-wave, (D) Averaged signal in at all 36 registration sites.

close as possible, right above the heart, starting from the jugulum (**Figure 5**). All points are aligned with this reference point with the help of a rigid grid pitch.

Having the SQUID detector in an unmovable position over the adjustable table for examinations, the patient was moved to each designed grid position (9 in total) without leaving the idle lying state.

The above-described measuring grid is the most widely used. There are other types of grids, in some grids, each point is set taking into account its own anatomical landmark.

The registration records were taken to collect data from each site for 30 seconds with 1 kHz sampling frequency while a 0.1–120 bandpass filter was applied. At the same time, the surface ECG lead II was registered. All the obtained data was written onto memory devices for later processing. It took from 7 to 8 minutes to measure each intended location.

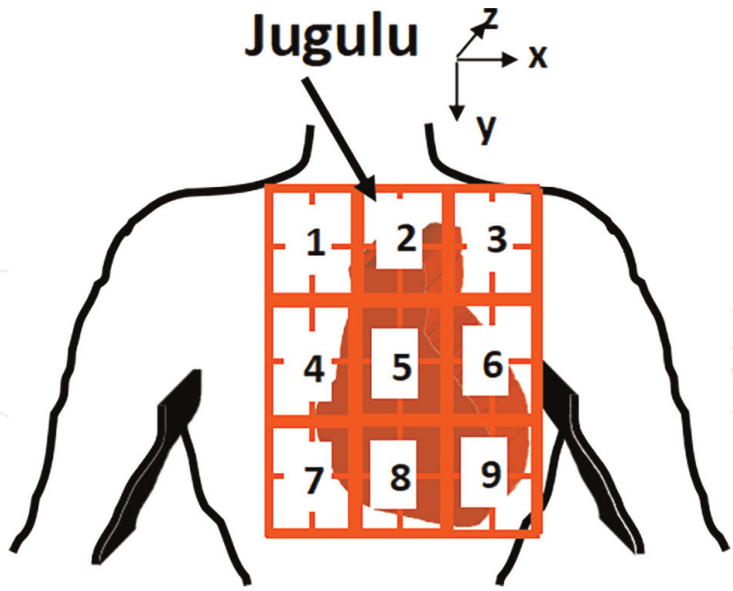

Figure 5.
A typical grid applied for getting the records, the precordial area covered has the dimensions 20 cm 20 cm. The starting point for the sensor is just higher the jugulum.*

4. The role of Electrophysiology for magnetocardiography

The ion current at cellular membranes in cardiac muscle cells defines their depolarisation and repolarisation. The latter also depends on single ions' temporally different permeability. Due to this, a shift arises in the membrane followed by changes in both the intra and extracellular volume currents. The spreading of these volume currents throughout the body causes the potential to alter the surface of the skin, so an electrocardiograph is able to detect the electrical potential changes once again. The nature and the functionality of the heart's specific cardiac conductivity system work in a way that it is electrically induced from the bottom state to the apex state. To apply the modeling for the heart's electrical activity, it can be substituted by a current dipole (also known as an equivalent dipole). Having the dipole with a distributed electrical field around it, the magnetic field should exist around it as well. The Biot-Savart approach helps to calculate the spatial dispersion induced by the dipole respectively. Here we define the magnetocardiogram as a recording of the frequent alternations in the magnetic field raising due to the cardiac cycle.

5. The MCG and the ECG key differences

Of course, MCG has similar morphological properties likewise ECG: we set a P-wave, a QRS complex, and T- and U- waves. Temporal correspondence between them is also most similar to ECG [7]. The majority of MCG devices make the magnetic field components measurement in a perpendicular way (radial or z-component) to the anterior chest (Bz). The key difference between dimensional layouts for ECG and MCG is their spatial alignment by 90° (**Figure 6**).

MCG is more sensitive to currents tangential to the chest surface, whereas ECG is more sensitive to radial currents.

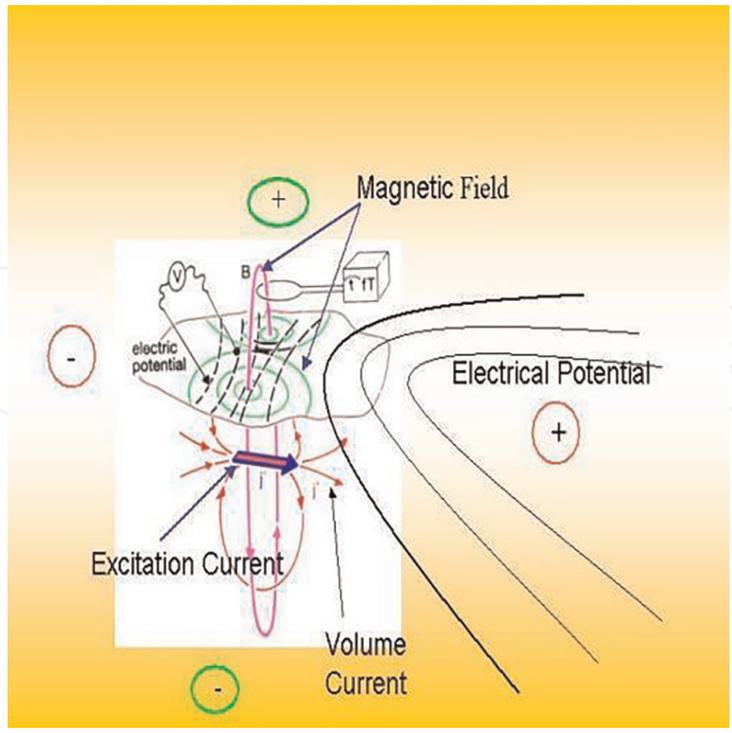

Figure 6.
Dimensional correspondence of electrical and magnetic fields.

Moreover, MCG is affected by isolated (vortex) current sources, which do not prevent any drops in potential on the body surface and thus the ECG is not able to detect them [8]. On the other hand, MCG is less influenced by conductivity alternations in the body (lungs, muscles, skin) than ECG. The MCG method does not invade the body at all, making the issues in the skin to electrode contact neglectable while being faced during the ECG. The switching in the ischemic diastolic TP and "true" ST switching is detected separately from each other by means of the direct-current MCG, due to the fact of missing potentials originating from the skin-electrode area.

6. Metrics and information technologies for the analysis of magnetocardiographic data based on two-dimensional visualization of the solution of the inverse problem of magnetostatics

The direct result of pre-processing of the data is 36 magnetocardiographic curves located at observation points—nodes of intersection of a rectangular grid, which is linked to the anatomical landmarks of the chest (**Figure 7**).

A detailed analysis of the morphology of MCG in healthy people was carried out. It was established that MCGs are similar to ECGs, recorded at the same points. The areas in which these or those elements of the MCG cardiac complex have the greatest amplitude have been analyzed. So, the wave P has the largest amplitude in the central zone of the upper half of the measuring grid corresponding to the V1 lead of ECG. The largest R—peak is recorded in the center of the measuring grid near the angle of the sternum, the deepest S-wave is in the left upper quadrant of the grid The deepest q is recorded in the upper left corner of the grid. In this area, the ventricle complex has the form qRs or qR. The complex Rs prevails in the right part of the grid. The ST segment is located close to the isoline at all registration points. The highest positive tooth T is

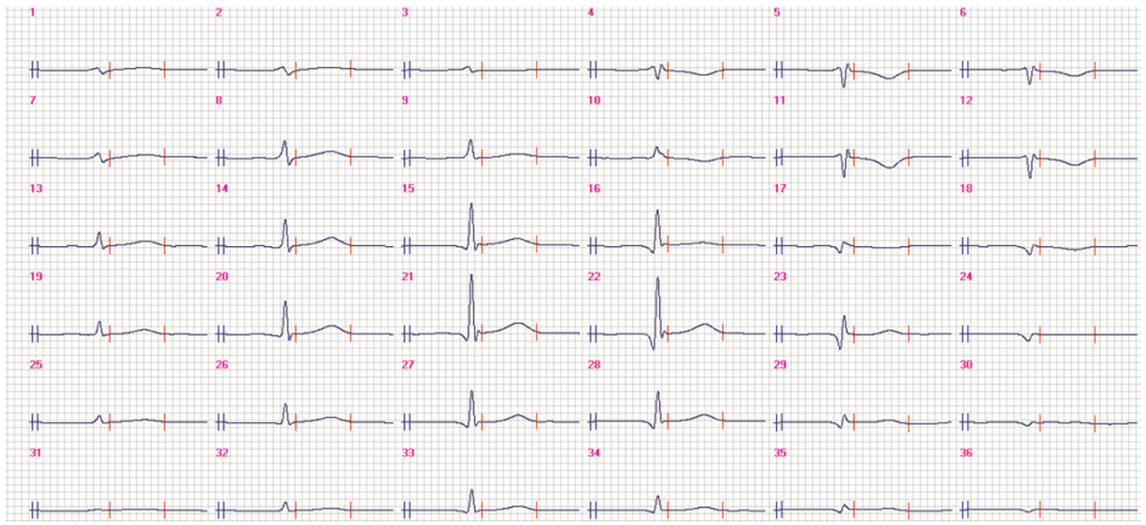

Figure 7.
36 MCG curves of healthy volonteer.

recorded in the same area as the largest R-peak, the deepest negative to this in the same area where the deepest S-wave is. The U-wave is always positive and best expressed in the left upper quadrant. The constitutional features of the normal MCG as well as features related to gender and age are also analyzed. It was found that men have significant differences in the magnitude of the QRS complex, depending on their age (up to 50 years the magnitude is higher), and growth (the higher growth, the greater the magnitude). In women, such differences are revealed in connection with weight—the more weight, the greater the magnitude. Totally for all categories, the coefficient of variation of the magnitude in healthy individuals is very high (0.48). This gives reason to doubt the advisability of applying criteria based on absolute values.

At the initial stage of development of magnetocardiography, the methods of its analysis copied the methods of analysis of electrocardiograms, the nomenclature of names of teeth, segments, and intervals developed for ECG analysis was used without changes. However, the analysis of individual MCG curves does not allow us to see the main advantage of magnetocardiography—high sensitivity to changes in the spatial distribution of the magnetic field at the points of the measurement plane and the associated density of ionic currents in the heart. This goal can be obtained after solving the inverse problem of magnetostatics.

This expression stands for the redesigning of the electrical activity in the heart using the recordings obtained above the surface of the human body. Since the measured magnetic field in MCG is found outside the very surface of the body and just over it, it is detected in a measurement surface from a short distance to the skin enclosing the chest cage.

Therefore, the next step in the analysis and interpretation of MCG data were methods closely related to the creation of modern information technologies.

For spatial fixation of data during MCG record the observation points are used. – These are nodes of intersection of a square grid. The magnetic signal is recorded at a frequency of 1 kHz. So the signal curve consists of individual "pieces" corresponding to individual "moments" of time. In other words, for each moment of time in 1 millisecond in points of a grid of measurements (6x6 points with a step of 40 mm on mutually perpendicular axes), it is possible to allocate simultaneously 36 values of a magnetic signal. If these signals are interpolated within the measurement area to a

more "frequent (with smaller distances between nodes)" grid, it is possible to construct a spatial distribution of the measured magnetic signal in the form of a magnetic field map. Thus, on the basis of 36 synchronous averaged MCG curves, two-dimensional (within 1 millisecond of time) magnetic field distribution maps are constructed using two-dimensional interpolation algorithms. Further, with the help of algorithms for solving the "inverse problem", equiinduction maps of the magnetic field distribution can be "converted" into the corresponding instantaneous maps of the distribution of current density vectors (CDV maps). A fundamental novelty of the proposed analysis of MCG data is the use of a new methodological approach—to assess the dynamics of changes in current density during the cardio cycle using maps sequentially arranged in time (dynamic mapping). This approach has identified a number of new MCG indicators, which, on the one hand, have a clear electrophysiological meaning, and on the other—to exclude the impact on research results of technical and design features of the MCG system used due to the analysis of relative values.

In the next stage, the analysis of the dynamics of the selected parameters of CDV maps in the selected time intervals of the cardio cycle (QRS, ST-T, Ta-e) with an arbitrary or specified time step (4–10 ms).

CDV instant maps and sets of such maps during cardio cycle intervals are the main diagnostic image and object of analysis in magnetocardiography. Each individual map, and even more so a set of cards during a certain phase of the cardio cycle, contains multifaceted information. Therefore, to take full advantage of the method for analysis, it is necessary to use not a single indicator, but their combination.

The following concepts define the classification of the CDV maps.

The electrical generator while being repolarized can be considered as an extended current origin placed at the borderline zone splitting excited and unexcited areas of myocardium. Having normal ventricular repolarization, this wave-front of excitation which is also integrated into a homogeneous conductivity medium has to be moved left-downwards within a 10°–80° sector. This model considers a couple of current types: the first one is known as "impressed current", since it is originated from "impressed" currents which are the transmembrane potential gradient and passive volume currents. On the other hand, put into homogeneous conductivity these volume currents contribute to two vortices, which are symmetrical and equivalent. The processed mapping has a dipolar layout closer to ideal (**Figure 8**) containing only one location with relatively larger vectors pointing left and downwards.

Green arrows display the "impressed currents", concentric-oriented curves represent current lines of the "volume" currents.

The appearance of inhomogeneity of conductivity due to some pathophysiological processes in the myocardium results in asymmetry and deformation of the vortexes (**Figure 9**), hence smaller portion of current vectors will be directed left-downwards.

Green arrows display the "impressed currents", concentric-oriented curves represent current lines of the "volume" currents.

Following the greater raise in abnormality, likewise, for ischemia issues, we monitor the appearance of the supplementary excitation wavefronts. These wave-fronts are pathological and definitely will represent the layout of maps with a non-dipolar structure (**Figure 10**). Thus, we encounter so-called supplementary locations (clusters) of current vectors. Usually, their directions are not pointed left and downwards, leading to the state where the amount of normally pointed vectors continuously drops. However, we do not neglect situations where the areas with supplementary vectors are pointed left and downwards. Anyways, these kinds of layouts should be named

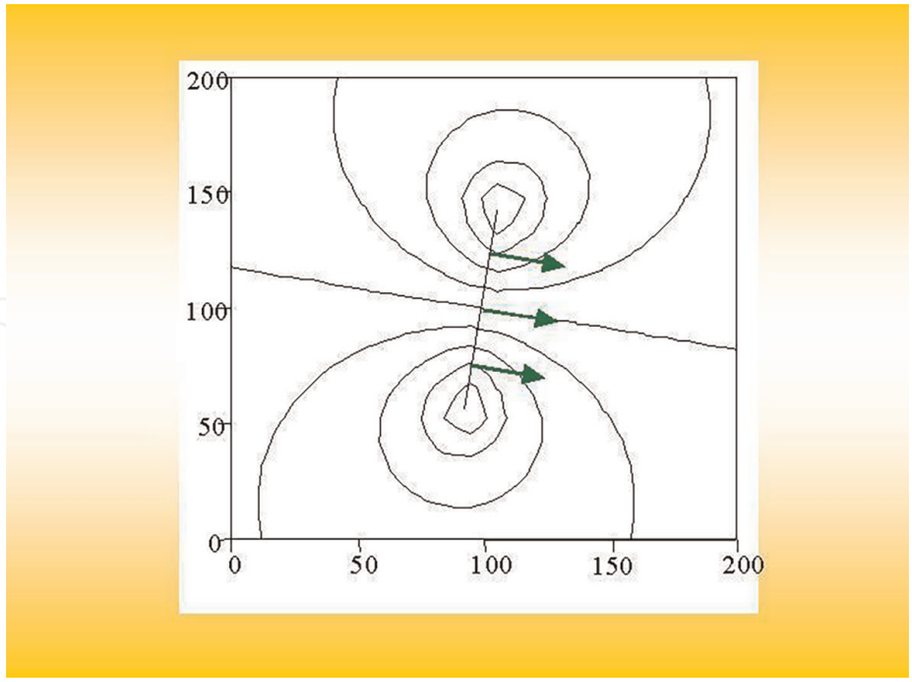

Figure 8.
The concept of current distribution in case of homogeneous conductivity.

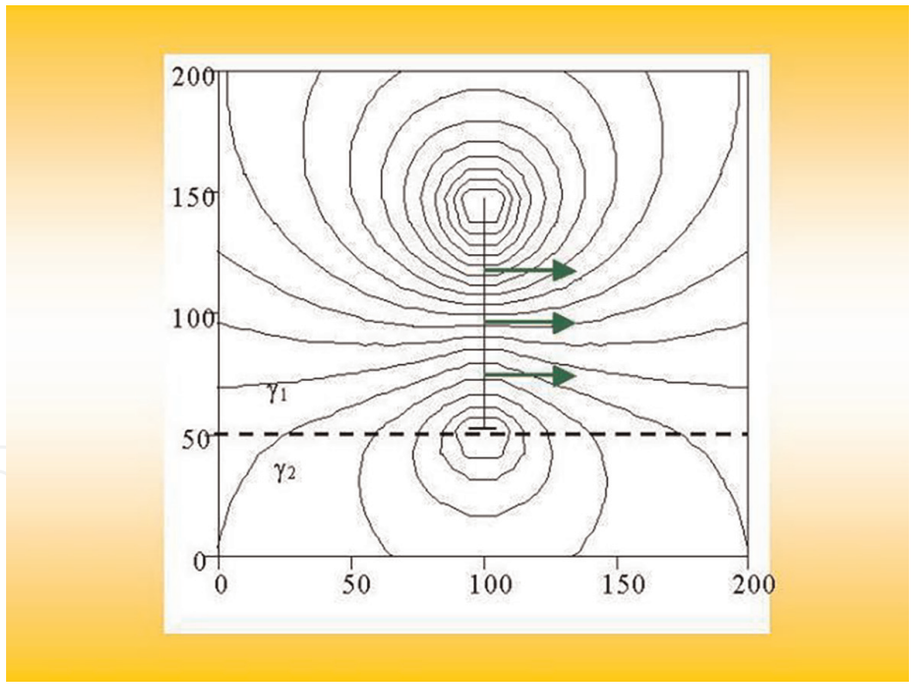

Figure 9.
Model of current distribution in the case of inhomogeneous conductivity (two zones with a ratio of conductivities $©_2/©_1=1/3$*).*

abnormal as well have given the decrease in homogeneity, i.e., the detection of supplementary areas (clusters).

Green arrows display the "impressed currents", concentric-oriented ´curves represent current lines of the "volume" currents.

Hence, the basic method of analysis of the spatial structure of the current distribution map is based on the concept of "proper" direction [9]. For each current

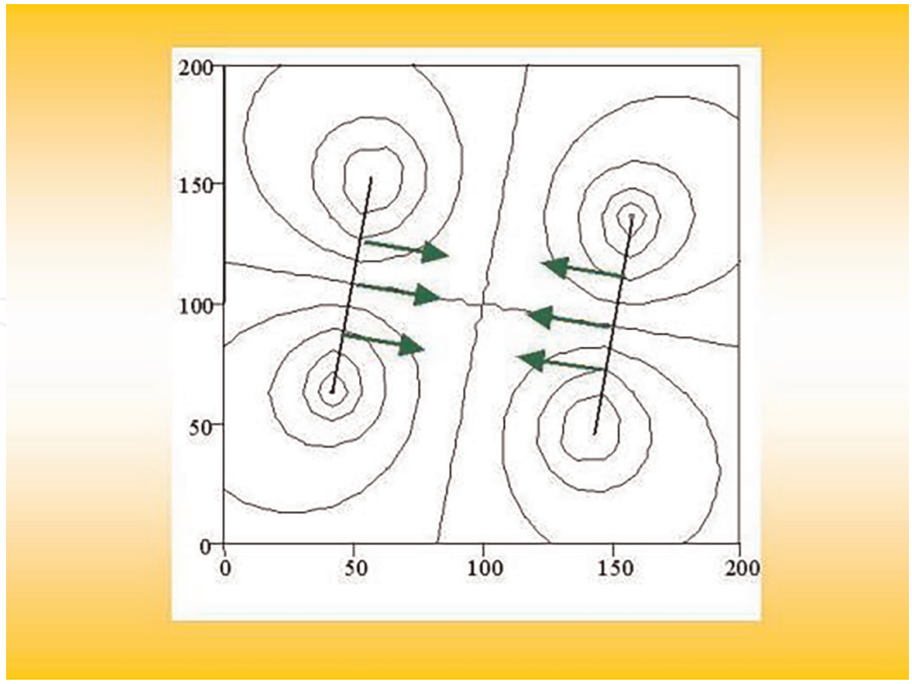

Figure 10.
The concept of current distribution with strong inhomogeneity (inhomogeneous conductivity (two excitation wavefronts of equal strength).

density vector, the normal direction is known, i.e., the sector within the pie chart from 0° to 180° and from −180° to 0°, which is used in the ECG, in which direction this vector is considered normal, i.e., "appropriate". In this case, the "proper" direction has a clear link to the interval of the cardio cycle to which this map belongs. Thus, during ventricular repolarization (from point J to the end of the T wave) the direction in the sector of 10°−80° is "appropriate". It is known that during ventricular depolarization, the excitation sequentially covers the interventricular septum, anterior-apical area, sidewall, and posterior-inferior region of the left ventricle. Each of these phases of depolarization has its own "proper" direction of current density vectors (**Figure 11a–e**).

The quantitative parameter of this type of analysis is a normalized 100% anomaly index (Abnormality Index—AI), i.e., the ratio of the sum of the lengths of vectors directed in the correct, "proper" for each time directly to the sum of lengths of vectors having different from the "proper" direction. From the electrophysiological point of view, this indicator reflects the ratio of ion fluxes flowing in the "proper" direction and in a direction different from the "proper" one. The next stage of the analysis is the assessment of the processes of de- and repolarization of the ventricles in general. The average AI values during the QRS complex—AIQRS total as well as during the ST-T interval—AISTT total is calculated.

Another group of indicators is designed to assess the homogeneity of the repolarization process—the similarity of the spatial structure of the maps and the smoothness of the curve of the total current (i.e., the curve consisting of arithmetic sums of values of all current density vectors for each instantaneous map during the studied interval).

To quantify the homogeneity of the spatial structure of maps over time, the correlation coefficient (similarity) score between all maps during the ST-T interval was proposed. To estimate the smoothness of the curve of changes in the total current, the shape of this curve is analyzed. The duration (in% to the total duration of the ST-T

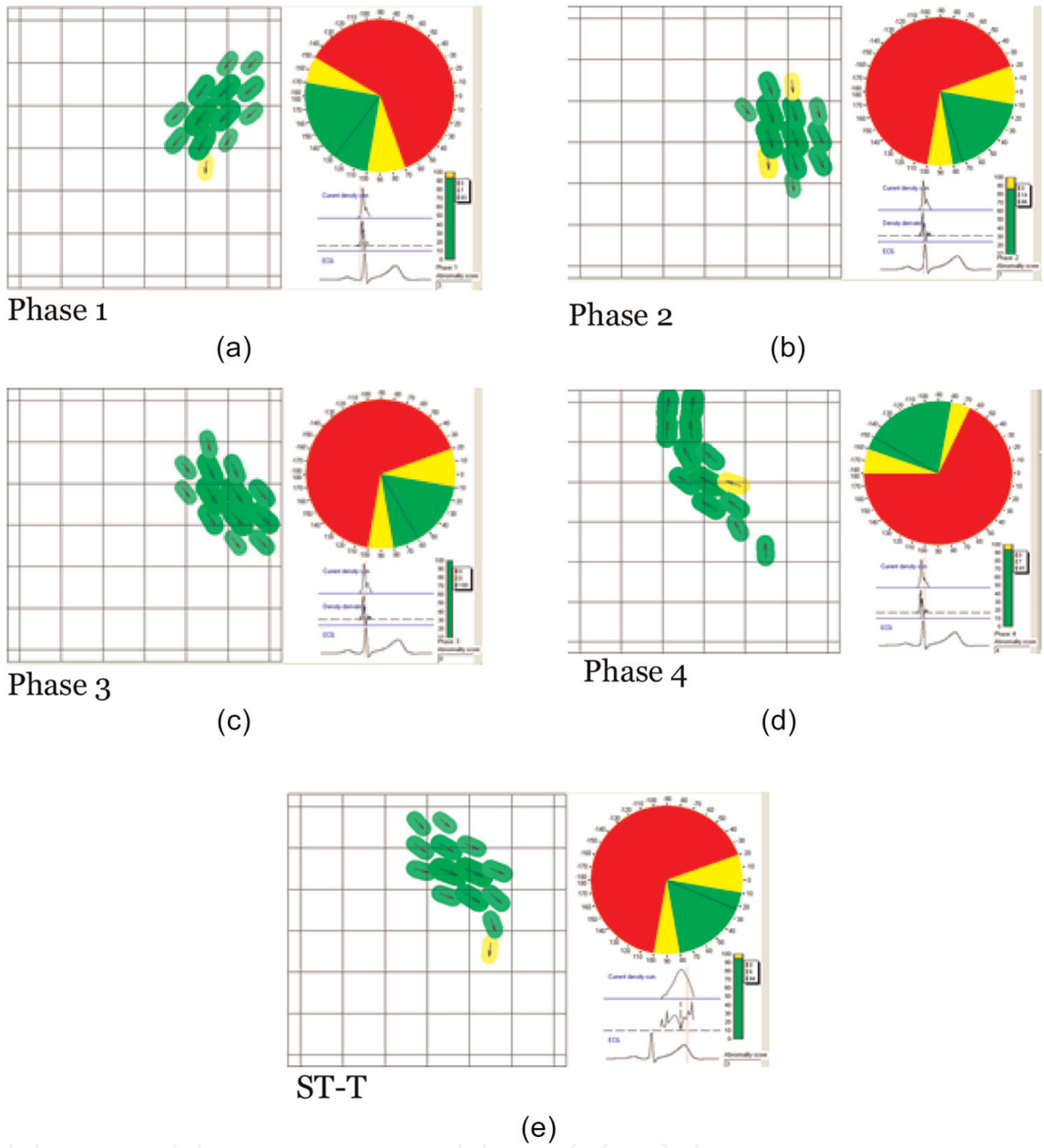

Figure 11.
Distribution maps of CDV of a healthy volunteer (left) and pie charts (right) of depolarization: a) interventricular septum (phase 1), b) anterior wall and apex of the left ventricle (phase 2), c)lateral wall of the left ventricle (phase 3), d) basal myocardium (phase 4), e) ventricular repolarization (ST-T).

interval) of the section of this curve from its beginning to the inflection point, i.e., to the moment of the beginning of its monotonic growth (ADur) is determined. The higher the Scor value and the lower the Adur value, the more similar the CDV maps are within the ST-T interval and the higher the homogeneity of the repolarization process as a whole. Decreases in similarity score values and increases in Adur almost always occur due to the changes at the initial part of the ST segment. The duration of one initial site corresponds to the time during which some areas of the myocardium are in a later phase of the transmembrane action potential compared to neighboring areas. In other words, the duration of this section reflects the degree of regional heterogeneity of repolarization.

Finally, the time dependence curve of the correlation coefficient of the current map with the map at the apex of the R wave during the ORS complex is investigated.

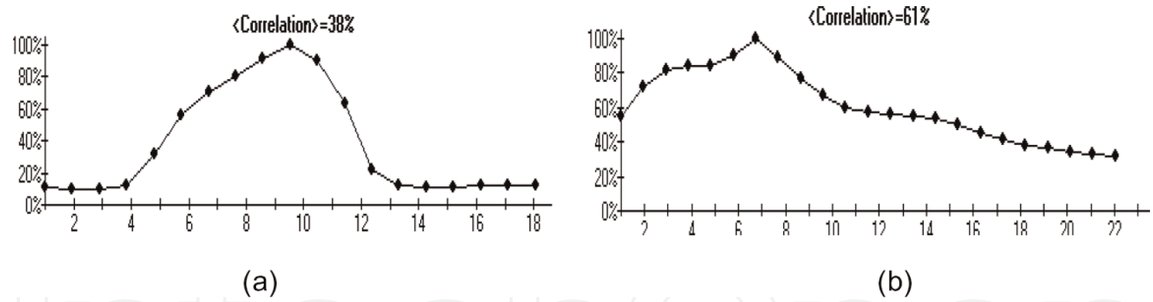

Figure 12.
Influence curves of the correlation coefficient of the current map with a map on the top of the tooth R: in healthy volunteer; b) in patients with a large MI.

In other words, the degree of similarity of each current map with the map at the top of the tooth R, i.e., with the map in which the value of the total current is greatest. The correlation coefficient between all maps during the QRS—CcorQRS complex is calculated. The shape of the correlation curve of the current map with the map at the top of the R wave is also analyzed. Normally, this curve has 3 characteristic inflection points (**Figure 12a**)—between the first phases of depolarization, the 2nd and 3rd phases, and 3th and 4th phases. In pathology, these points, especially 1 and 3 are smoothed or completely absent (**Figure 12b**).

The calculation of the above set of temporal and spatial features is based on a key electrophysiological concept—the increase of electrical heterogeneity (heterogeneity) of the myocardium in the occurrence of pathological processes, such as ischemia.

In our opinion, one of the main ways to increase the functional efficiency of magnetocardiography is to build systems for automatic classification of magnetocardiograms based on the ideas and methods of machine learning and pattern recognition.

We have developed a method for analyzing CDV maps during ST-T intervals based on pattern recognition.

Correlation analysis was used to classify each current density map. The main idea of the method of current density distribution map classification based on correlation analysis is to find and compare the correlation coefficients of the map under analysis with each of the maps in the reference set. Reference sets consist of pre-classified by the doctor current density distribution maps, each of which belongs to one of the groups corresponding to a certain state of the cardiovascular system. For each of the classified maps, the correlation coefficients of the vector of values and the vector of directions with the corresponding vectors of each of the maps from the reference set are calculated as follows [10]:

$$\begin{aligned} r = \sum ni = 1(xi - x^{\overline{}})(yi - y^{\overline{}}) \sum ni = 1(xi - x^{\overline{}})2\sqrt{\sum ni} \\ = 1(yi - y^{\overline{}})2\sqrt{(1)}r = \sum i = 1n(xi - x^{-})(yi - y^{-}) \sum i \\ = 1n(xi - x^{-})2\sum i = 1n(yi - y^{-})2 \end{aligned} \quad (1)$$

Where n is the dimension of the vectors, for our case n = 100,

x_i, and y_i are values of vectors for which the correlation coefficient is calculated and $x^{-}x^{-}$, and $y^{-}y^{-}$are the mean values of the vectors, calculated as follows:

$$x^{-} = 1n\sum i = 1nxi(2)x^{-} = 1n\sum i = 1nxi \quad (2)$$

$$y^{-} = 1n\sum i = 1nyi(3)y^{-} = 1n\sum i = 1nyi \tag{3}$$

After that, the values of the obtained correlation coefficients for two vectors are multiplied; thus, the resulting correlation coefficient is obtained, which takes into account both the modulus correlation and the direction of the current density vectors. As a result, a set of the resulting correlation coefficients with the maps of each group of the reference set is obtained for each map. After that, an array of m maximum values of the resulting correlation coefficient is formed for each group, and their average value is found. Thus, for each CDDM we obtain a set of key-value pairs with the groups corresponding to the state of the cardiovascular system as keys, and the above described average values of the maximum correlation coefficients as corresponding values. The maximum of these values indicates the group to which the map of the distribution of the current density to be classified should be assigned. The best result was obtained for m in the range of 1–5, and the accuracy of classification in these cases is highest and does not significantly depend on the number of maximum values; therefore, in this study, we use m = 3.

One of the methods for pattern classification is the k-nearest neighbor (k-NN) rule. It classifies each unlabeled object according to the majority label of its k-nearest neighbors in the training set. Despite its simplicity, the k-NN rule often yields competitive results and in certain domains, when cleverly combined with prior knowledge, it can help to solve even quite difficult classification tasks.

The result of k-NN classification depends significantly on the metric used to compute distances among different feature vectors. In [11], it was shown that using different distances for k-NN classification gives an opportunity to decrease the error rates for different classification problems, such as face recognition, spoken letter recognition, and text categorization. It was also demonstrated that a k-NN classifier with a correctly chosen distance metric shows better results, even when compared to SVM used for same classification tasks.

In this study, the three most commonly used metrics, which are special cases of Minkowski distance, Eucledian, Cityblock, and Chebychev, were examined. Let us consider X as a 1-×-32 feature vector of a classified CDDM and Y as a feature vector of each CDDM in the training set. In our study, binary classifiers with three different distance metrics were developed. A classifier with an Eucledian metric distance between two points Xs and Yt, whose coordinates are values of X and Y, respectively, is defined as follows:

$$d2st = (xs - yt)(xs - yt)'(4)dst2 = (xs - yt)(xs - yt) \tag{4}$$

For Cityblock (also known as Manhattan) metric:

$$dst = \sum j = 1nxsj - ytj(5)dst = \sum j = 1n|xsj - ytj| \tag{5}$$

where n is the size of vectors X and Y, and in our case n = 32–number of features.

For Chebychev metric:

$$dst = \{xsj - ytj\} \tag{6}$$

2142 current density distribution maps were analyzed, which were assigned to 6 different groups depending on the verified diagnosis of the patient. These maps amounted to 6 basic databases of reference images. Each of these databases includes maps that are most specific to a particular disease.

Group	1	2	3	4	5	6	7	8	9	10	11	12	13	14	15	16	17	18	19	Mean1	Mean2
Athlet's heart	10.3	6.5	4.59	4.49	3.19	5.27	8.04	10.16	15.21	19.51	26.47	32.67	39.56	37.28	37.48	33.9	33.6	28.94	24.68	20.1	0
Norm	6.93	7.16	6.28	5.99	5	3.82	6.44	6.35	12.71	17.52	26.68	35.07	43.81	45.41	43.83	43.04	43.32	40.83	40.18	23.18	22.81
LVH 1	3.22	2.15	1	0.75	0.78	1.39	6.59	5.9	5.94	6.77	9.63	13.75	18.12	16.03	16.68	19.36	19.98	25.08	21.35	10.24	0
LVH 2	1.67	2.23	3.28	2.72	2.98	2.35	5.89	5.39	6.75	8.06	11.95	15.53	20.23	19.96	19.49	18.68	19.17	22.66	20.74	11.04	0
LVH 3	5.64	5.54	4.49	3.03	2.01	2.24	8.12	8.94	11.17	12.63	13.05	12.74	12.95	10.26	10.6	9.45	9	9.55	7.85	8.38	0
Non-coronarogenic diseases	7.85	8.71	9.67	8.94	8.98	8.21	11.59	12.83	17.21	20.82	28.01	35.18	36.62	42.53	43.17	40.95	41.26	33.61	38.56	23.93	0
Microvascular disease(M)	15.19	12.9	15.08	13.47	13.99	10	10.52	13.51	16.27	19.6	23.09	25.46	27.01	26.2	24.3	21.91	21.93	18.41	17.24	18.22	3.9
Myocardial damage	3.29	5.93	4.46	3.17	2.44	3.11	6.25	3.17	1.73	2.26	3.67	6.65	10.22	10.7	10.63	10.35	10.86	12.26	9.67	6.36	0
CAD 1	14.45	21.56	32.26	33.32	37.86	34.46	36.52	37.33	38.3	39.23	41.63	42.85	42.48	44.74	45.47	43.6	44.2	40.26	43.3	37.57	73.29
CAD 2	4.33	5.34	4.19	4.34	3.36	6.51	7.7	7.87	6.78	5.92	4.78	4.51	4.67	5.14	5.42	5.5	5.8	5.62	5.11	5.42	0
CAD 3	7.39	10.47	10.53	9.91	9.59	10.83	11.21	11.52	9.18	8.49	2.89	3.82	5.19	7.14	6.83	8.14	8.19	7.86	10.21	8.39	0
CAD 4	6.54	3.37	2.38	1.99	1.32	2.5	4.04	3.83	4.27	3.86	6	8.61	11.63	12.23	13.29	13.33	13.44	13.19	12.47	7.28	0
CAD 5	3.88	7.61	8.06	5.96	5.95	2.29	5.33	4.05	3.18	2.05	1.37	1.17	1.14	1.46	1.63	1.82	1.85	2.24	2.94	3.37	0

Figure 13.
Correlation coefficients for the consecutive CDV maps relative to the reference base of maps for each of the 14 categories.

These groups are as follows: normal, left ventricular hypertrophy (LVH), non-coronary heart disease, microvascular disease, myocardial infarction, and coronary heart disease (coronary heart disease) other than MI. In turn, the norm group is divided into 2 subgroups, the LVH group—into 3 subgroups, and the coronary heart disease group—into 6 subgroups. Thus, in the end, we have 14 categories. Correlation coefficients were calculated for the current map relative to the reference base of maps for each of the 14 subcategories.

Next, the results of the classification of individual consecutive maps on the ST-T interval were averaged for the entire ST-T interval. As a result, we obtain the probabilities of belonging to a particular magnetocardiographic examination in each of the 14 categories for each MCG examination (**Figure 13**).

In this case, the highest probability of belonging to the category of coronary heart disease, subcategory 1

7. Clinical approbation of metrics of analysis of magnetocardiographic data on the basis of two-dimensional visualization of the solution of the inverse problem of magnetostatics. Multicenter studies

The purpose of using any diagnostic parameter is to formulate a clinically significant diagnostic conclusion, i.e.:

a. decision on the presence or absence of a pathological process;

b. in the case of a process—determining the severity.

The set of features has higher diagnostic accuracy than a single feature. Thus, there is a problem with forming from a set of parameters of a single complex indicator, which synthesizes various aspects of the information contained in each individual indicator. Such an indicator can be created on the basis of the method of linear discriminant analysis (LDA). As a result, a discriminant function is automatically built. If the value of the function is greater than the threshold, the results of the MCG test are positive, if less—negative.

Another, empirical-statistical approach, which is used to form a comprehensive index, is calculated on the basis of scores. When using this approach, the values of all quantitative indicators are a priori divided into ranges. When the value of an individual indicator falls into the appropriate range, it is given a certain number of points.

Then the number of points of all indicators is summed. If the sum of points exceeds a certain threshold, the MCG test is considered positive, if on the contrary—negative. If the test is positive, the number of points determines the severity of the pathology on the principle—the higher the score, the more pronounced the pathology. Such scores are widely used in electrocardiography (Sylvester score, Freuleher score, CIIS and others), as well as to assess the results of the test with dosed exercise (Duke's index). We have created an integrated scoring criterion of the additive type for the diagnosis of myocardial ischemia using MCG. The value of this criterion was recently investigated by us in two multicenter studies involving foreign colleagues. A two-center study was conducted at the National Military Medical Clinical Center and at the Catholic Clinical Philippusstift (Essen, Germany) [12]. We examined 79 patients with complaints of chest pain and normal or non-informative results of ECG and echocardiography at rest, i.e., in difficult-to-diagnose cases. All patients underwent coronary ventriculography. According to the results of coronary angiography, patients were divided into subgroups with stenosis> 70% in at least one of the main coronary arteries (subgroup 1a) and a subgroup of persons without hemodynamically significant stenosis (subgroup 1b). Control group 2 consisted of 30 healthy volunteers close in age. **Table 1** shows the indicators of diagnostic value of the complex MCG index to detect significant stenosis of the coronary arteries in difficult-to-diagnose cases.

The goal of any diagnostic test is to reduce the uncertainty level and to increase the confidence of the investigator in valuable decision-making. The present study investigates a group of patients for whom this decision is performed on the basis of coronary angiography. The pretest probability of hemodynamically significant coronary artery stenosis in patients analyzed was about 50%; therefore, the degree of uncertainty is the highest in this case. Post-MCG probability to use analogous to post-ECG probability that a hemodynamically significant stenosis is absent is 85% in the case of negative result of MCG-study. In the case of a positive MCG result, the probability of haemodynamically significant stenosis is 93%.

Thus, the results of our MCG-study reduce uncertainty in decision-making. Coronary angiography should be considered for patients with positive MCG-results. In the case of negative MCG-results, the invasive procedure could be avoided.

An even larger multi-center study was conducted in three leading clinics in Beijing under the guidance of specialists from the main hospital of the Chinese Navy. A total of 133 people were examined (mean age 59 $\pm$ 3.1 years). All surveyed individuals were divided into three groups. The first group (61 people) consisted of patients with severe myocardial ischemia who met the criteria for revascularization: the degree of coronary artery stenosis was ≥80% or was between 50% and 80%, with a margin of coronary blood flow ≤0.8.

Diagnostic value parameters	**Comparison of subgroups 1a и 1b**	**Comparison of subgroup 1a with subgroup 2**
Sensitivity, %	93	93
Specificity, %	84	94
PPV, %	85	94
NPV, %	93	93

Table 1.
Diagnostic value of complex MCG index.

The second group (13 people)—patients whose myocardial ischemia is confirmed by the "gold standard"—invasive coronary angiography but has not yet met the criteria for revascularization. The third group (59 people) is the control group. The percentage of coincidence of ICG results and coronary angiography in each group was as follows: for severe coronary heart disease—85.45%, for mild coronary heart disease —77.78%, in the control group—87.10%.

Achieved a total sensitivity of 93.75%, a specificity of 87.10%, PPS was 88.24%, and NPV 93.10%.

Thus, magnetocardiographic examination is a reliable method of diagnosing chronic coronary heart disease, including in difficult-to-diagnose cases.

Analyzing the possibilities of using different methods for myocardial ischemia detection, it is necessary to take into account their position on the steps of the "ischemic cascade". For example, systolic myocardial dysfunction, which is detected by echocardiography under load, in the ischemic cascade manifests itself later than the heterogeneity of blood flow. Manifestation of myocardial ischemia in the form of changes in the ST segment on the ECG is manifested even later and therefore the possibilities of the ECG in the detection of myocardial ischemia, even under load, are limited. At the top of the ischemic cascade is the anginal syndrome. What is the place of the MCG in this context? In our opinion, in some cases, the ICG at rest is outside the ischemic cascade, recording the "history" of episodes of past myocardial ischemia that have occurred before. The rather high sensitivity of the MCG is due to the fundamental physical advantages of the method. The rather high values of diagnostic accuracy of MCG received in numerous research are reached at rest. The causes of electrophysiological changes at rest in patients with coronary heart disease are diverse. First of all, these are changes in repolarization as a result of apoptosis. Also, previous episodes of myocardial ischemia can lead to cell necrosis in limited areas of the myocardium, causing impaired electrogenesis. Several articles have shown that transient ischemia contributes to an increase in interstitial endocardial fibrosis in patients with a history of MI. It is also suggested that in coronary heart disease already at rest there is a significant alternative to the level of myocardial blood supply. This in turn can also lead to subtle electrophysiological changes that are already taking place at rest.

It is known that myocardial ischemia is accompanied by activation of free radical processes, and it is obvious that this should be manifested by disturbances in the functioning of ion channels, changes in TPD, and excitability of conductive cells and cardiomyocytes. It can be assumed that changes in MCG parameters in patients with coronary heart disease at rest are due to changes in electrophysiological characteristics such as resistance of membranes and intercellular connections, and the rate of conduction.

That is, we can conclude that due to its high sensitivity, the MCG at rest reveals the effects of episodes of transient ischemia (apoptosis, interstitial fibrosis, inhomogeneity of perfusion, and metabolism) [13].

Sufficiently high sensitivity of MCG is caused by fundamental physical advantages of the method. The result of these physical advantages is that the MCG signal more completely and accurately reflects electrical processes of the heart. MCG is much more sensitive than ECG to myocardial ischemia, thus MCG signal is changed even in cases when the shape of the ECG signal does not differ from normal. This advantage of MCG most clearly could be demonstrated by the shift of ST-segment (**Figure 14**).

Figure demonstrates standard ECG and MCG, registered on the same day almost simultaneously. There are no ST-segment shifts registered in any of the ECG leads. On the contrary, at points 14 and 20, there is a depression of ST-segment, and at points 4,5, and 6—an elevation of it.

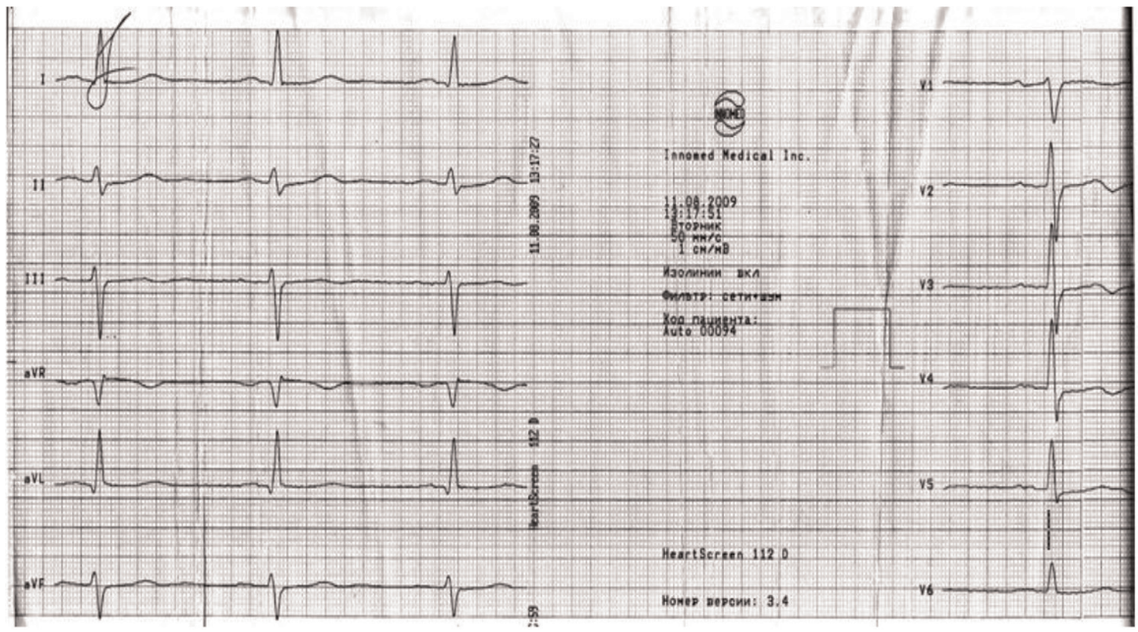

(a)

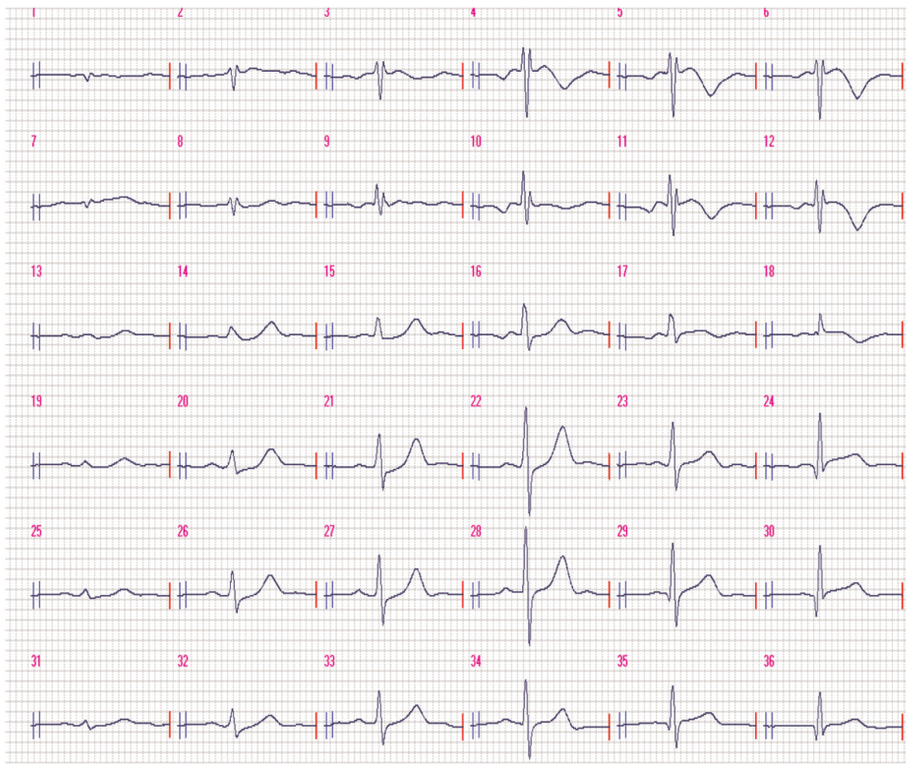

(b)

Figure 14.
ECG in 12 leads (A) and MCG (B) of the patient with 2 vessels CAD (high-grade RCA and LCX stenosis).

It is important to understand that the presence of depression and elevation simultaneously within the 36-point MCG grid has the same electrophysiological basis as reciprocal changes in ST-T interval of ECG leads. In the case above, there is an ST depression in the right-central quadrant of grid (points 14,20) and elevation in left-upper quadrant of MCG grid. In our opinion, this configuration may reflect ischemia of the inferior wall of the left ventricle. Naturally, the identified dislocations of the ST

segment will clearly appear on the CDV maps throughout this segment. We have developed the atlas of representative current density maps within ventricular repolarisation we have seen in patients with different variants of chronic CAD. We have selected "difficult-to-diagnose" patients with normal or uncertain, non-specific results of the routine tests. In that way, we would like we wanted to highlight the role of MCG in clinical routine—to feel out the gap between routine but non-sensitive diagnostic methods and much more expensive advanced non-invasive and invasive techniques [14].

8. Metrics and information technologies for the analysis of magnetocardiographic data based on three-dimensional visualization of the solution of the inverse problem

The original advanced method to solve the inverse problem of magnetostatics based on the results of measurements of the magnetic heart signal was developed recently. As the first step, a model of a point source of magnetic field (i.e., magnetic dipole) was used. The location and magnetic moment vector of magnetic dipole uniquely defined by known (measured) values of magnetic field at given points in space [15]. In the subsequent stages of data processing and conversion, other models of the signal source are also used. For example, the source of the magnetic field can be represented as a set of N different magnetic dipoles distributed in the volume of the heart [16]. In this case, the results of measurements of the magnetic field to determine the location of several signal sources are distributed as independent in the three-dimensional volume of the human heart. A model of a flat system of "currents" (distribution of the current density vector) is used for spatial analysis of the magnetic cardio signal and its sources. It is assumed that in space the selected plane, which is parallel to the plane of measurement, is secant with respect to the volume of the heart and is located at a given distance from the plane of measurement. In the proposed Primin and Nedayvoda algorithm, the coordinate of the plane with signal sources is a variable and its value is also determined by the measurements of the magnetic field—as the value of the z-th coordinate of the dipole source, which was determined at the previous stage of MCG signal processing. The problem for a planar current system is based on the application of the double integral Fourier transform and takes into account the spatial configuration of the magnetic flux transformer SQUID gradientometer [17]. An algorithm for converting information to solve the inverse problem was developed in the case if the results of measurements of the magnetic cardio signal need to determine the values of current density vectors in a given set of slices ("layers") [18]. Each of the layers is located in a plane parallel to the measurement plane, the coordinates ("depth") of each layer are set either with a given step (uniform distribution) or discretely based on the results of solving the inverse problem obtained in the previous stages (non-uniform distribution).

The power distribution of the current density vector is presented in the form of a so-called polar diagram. The principle of plotting is based on the segmentation scheme adopted as a standard in the analysis of measurement results in computed tomography and ultrasound of the heart [19]. Software implementation assumes that the three-dimensional surface consists of 5 segments: 1—anterior, 2—lateral, 3—inferior, 4—septal, and 5—apical.

Three-dimensional imaging methods have been successfully used to solve several important clinical problems, including, for example, determining the viability of the

affected areas of the myocardium in patients with various forms of coronary heart disease. Thus, a fairly high level (74%) was found between the contractility of the segments of the anterior wall of the left ventricle and the current density in this area of the myocardium in patients with chronic coronary heart disease [20].

9. Myocardial damage in patients recovered from COVID-19

2 years ago, a new challenge for humanity emerged—Covid-19 pandemic. It has led to well over 200 million infections, with a fatal outcome in over 4.5 million cases. Of the survivors, the majority showed long-haul symptoms – now often called Long COVID [21].

One of the important long-term clinical consequences of COVID-19 seems to be heart damage [22]. Signs and symptoms of possible heart damage after COVID-19 may include severe fatigue, palpitations, chest pain, shortness of breath, and postural orthostatic tachycardia syndrome (POTS) due to neurologic disturbances, post-exertional fatigue, and higher troponin levels.

In addition, heart inflammation appears to be prominent in COVID-19. This might involve both the myocardium and the pericarditis, causing severe fatigue without other obvious symptoms. The diagnosis of myocarditis is relatively inaccurate because both tests and diagnostic protocols are lacking precision. The course of the illness is therefore unknown at present, but some early reports have shown that symptoms lingered for a median of 47 days before diagnosis was accomplished by cardiac magnetic resonance (CMR) imaging [23].

Magnetocardiography, due to its high sensitivity is a potentially valuable method to detect the signs of myocardial damage in patients with COVID-19.

Therefore, 59 patients (mean age 42 ± 3.9 years) who recovered from COVID-19 were examined as it was shown in section 2 of this chapter in the Main Military Hospital of Ukraine and in the 8th People's Hospital of Guangzhou. This group was divided into two subgroups depending on the time elapsed since recovery: 1–3 months after recovery (11 patients) and 7–10 month after recovery (48 patients). 78 healthy volunteers constituted the control group. These persons were examined earlier, in 2017–2018.

The method of data analysis was based on pattern recognition (see section 5 of this chapter). The probabilities of CDV maps within ST-T interval belonging (i.e., correlation coefficients) to six basic databases of reference images have been calculated. Each of these databases includes maps that are most specific to a particular disease. Then, the rank of category called "Non-coronary Heart Diseases" was determined. This rank (i.e., the relative value of the correlation coefficient) could be from 1 to 6.

To evaluate the difference between the examined groups, non-parametric Wilcoxon—Mann—Whitney test, designed to assess categorical variables, was used (**Table 2**).

There is a highly statistically significant difference between the rank of CDV maps, which belongs to the category "Non-coronary Heart Diseases" between the group of

Patients, recovered from COVID-19, total M±m, n = 59	**1–3 month after recovery M±m, n = 11**	**7–10 month after recovery M±m, n = 48**	**Control group M±m, n = 78**
3.78 ± 1.46*	2.27 ± 1.67*	4.08 ± 1.42	4.43 ± 1.25

** $p \leq 0.05$ in comparison with control group.*

Table 2.
The rank of category "Non-coronary Heart Disease" in groups examined.

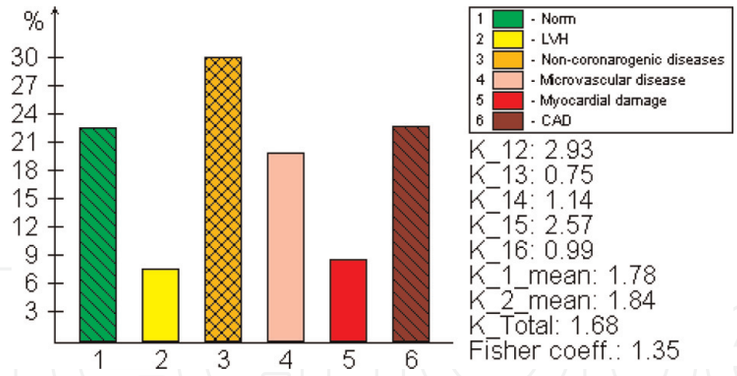

Figure 15.
A diagram, showing the average correlation coefficients of CDV maps with 6 basic databases of reference images in a 61-years patient who has recently recovered from COVID-19. The highest correlation with the "Non-coronary Heart Diseases" category is observed.

patients recovered from COVID-19 and the control group. In patients, who recovered from COVID the signs of non-coronary heart diseases are much more pronounced, than in the control group. This is especially true for recently recovered patients, within 1–3 months before MCG-examination (**Figure 15**).

At the same time, the differences between the group of patients, who recovered from covid relatively long ago and the control group take place only at the level of a tendency ($p \leq 0.25$).

Note that all examples of the application of the new metric for the analysis of subtle changes in the magnetic field of the human heart are critical parts of the relevant new diagnostic technologies.

The meaning of the development and implementation of any new diagnostic technology is to solve difficult diagnostic problems that are difficult to solve with existing methods. The above examples of new metrics developed by us fully meet the criteria for solving a complex diagnostic problem in cardiology, and in the first place, there is a wide range of differential diagnosis and low availability and/or high cost of diagnostic methods already included in existing clinical guidelines on this problem. In addition, it should be noted that a key sign of the maturity of the new technology is the presence of certificates of conformity issued by the authorized department of a country, as well as patents confirming its novelty. In this context, it should be noted that in addition to national certificates and patents, our proposed metrics as a result of careful long-term testing of the most modern procedures and received the relevant international certificates and patents for inventions. This is a guarantee of further intensive use of the unshielded magnetocardiography in medical practice at the international level.

The emerging diagnostic technology regarding existing ones might play one of the three future roles: replacement, triage or adds one [24]. At present, magnetocardiography can play the role of triage and supplementation among well-established methods for diagnosing myocardial damage of various origins. Further development of the method requires further, larger multicenter studies involving several dozen clinics in different countries.

10. Conclusions

1. The development of new information technologies and metrics based on magnetocardiography for the analysis of small changes in biological signals is a

modern technological trend that improves the accuracy of many diagnostic methods, including methods of analysis of electrical activity of the heart.

2. New magnetocardiographic metrics for the analysis of the spatial structure of 2D magnetocardiographic current density distribution maps allow to diagnose myocardial ischemia with high accuracy, which has been proven in the course of intercenter studies.

3. Metrics based on three-dimensional visualization (polar diagram) of the electrical activity of the ventricles of the heart on the basis of magnetocardiographic data provide an opportunity to solve important clinical problems, in particular to determine the viability of affected myocardial infarction in patients with various forms of coronary heart disease.

4. New metrics for 2D magnetocardiographic current density distribution maps analysis, based on pattern recognition allow to detect signs of myocardial damage in patients, who recently recovered from COVID-19. Further, larger studies are needed to confirm these findings.

Acknowledgements

The authors want to express their sincere gratitude to outstanding experts in physics, mathematics, cryogenic engineering Drs. Michael Primin, Volodymyr Sosnytskyy, Pavlo Sytkovy, Igor Nedayvoda, Yury Minov, Pavlo Shpylevoi, Mykola Budnyk, Yury Frolov from Glushkov Institute for Cybernetics of NAS of Ukraine as well as Dr. Anton Popov and Eugen Udovichenko from National Technical University of Ukraine "Igor Sikorsky Kyiv Polytechnic Institute". In addition, the authors warmly thank the great teams of leading hospitals in Ukraine, China, and Germany, with whom they were lucky to productively cooperate.

Special thanks to Mr. Bin-Zhen Zhang from North University of China, Mrs. Wei-Wei Quan from Ruijin Hospital affiliated to Shanghai Jiaotong University, as well as Mrs. Xiang-Yan Kong from Ningbo University for their outstanding efforts aiming to develop MCG-technology in China.

Author details

Illya Chaikovsky[1*], Anatoly Kazmirchyk[2], Sergey Sofienko[2], You-Bin Liu[3], Ya-Feng Zhou[4], Xie Feng[5], Lin Xu[5] and Yan-Fei Huang[5]

1 Glushkov Institute for Cybernetics, Kiev, Ukraine

2 National Military Medical Clinical Center (MMCH), Kiev, Ukraine

3 8th People's Hospital of Guangzhou, Guangzhou, China

4 Suzhou Dushu Lake Hospital, Suzhou, China

5 Suzhou Cadiomox Ltd, Suzhou, China

*Address all correspondence to: illya.chaikovsky@gmail.com

References

[1] Benjamin EJ, Virani SS, Callaway CW, Chamberlain AM, Chang AR, Cheng S, et al. Heart disease and stroke statistics–2018 update: A report from the American Heart Association. Circulation. 2018;**137**(12): 67-492

[2] Simoons ML, Hugenholtz PG. Estimation of the probability of exercise in duced ischemia by quantitative ECG analysis. Circulation. 1977;**56**:552-559. DOI: 10.1161/01.CIR.56.4.552

[3] Gerhard B, Richard M. Detection of the magnetic field of the heart. American Heart Journal. 1963;**66**(1):95-96

[4] Chaikovsky I, Lutay M, Sosnitsky V, et al. Ventricular repolarization disturbances diagnostics in chronic ischemia patients evidence derived from MCG. In: Biomag 96: Proc of 10th International Conference on Biomagnetism. 1999. pp. 444-447

[5] Chaikovsky I, Kohler L, Hecker T, Hailer B. High sensitivity of magneto cardiography in patients with coronary artery disease and normal or unspecifically changed ECG. Circulation. 2001;**102**(18):791

[6] Cohen D, Edelsack EA, Zimmerman JE. Magnetocardiograms taken inside a shielded room with a superconducting point-contact magnetometer. Applied Physics Letters. 1970;**16**(7):278-280. DOI: 10.1063/1.1653195

[7] Koch H. Recent advances in magnetocardiography. Journal of Electrocardiology. 2004;**37**:117-122. DOI: 10.1016/j.jelectrocard.2004.08.035

[8] Dutz S, Bellemann ME, Leder U, Haueisen J. Passive vortex currents in magneto- and electrocardiography: Comparison of magnetic and electric signal strengths. Physics Medical Biology. 2006;**51**(1):145-151

[9] Chaikovsky I. Magnetocardiography in unshielded location in coronary artery disease detection using computerized classification of current density vectors maps. 2006

[10] Udovychenko Y, Popov A, Chaikovsky I. Multistage classification of current density distribution maps of various heart states based on correlation analysis and k-NN algorithm. Frontiers in Medical Technology. 2021:3-11

[11] Udovychenko Y, Popov A, Chaikovsky I. k-NN binary classification of heart failures using myocardial current density distribution maps. In: Signal Processing Symposium (SPSympo). 2015. pp. 98-102

[12] Chaikovsky I, Hailer B, Sosnytskyy V, Lutay M, Mjasnikov G, Kazmirchuk A, et al. Predictive value of the complex magnetocardiographic index in patients with intermediate pretest probability of the chronic CAD: Results of a Two-Center Study. Coronary Artery Disease. 2014;**25**(6):474-484. DOI: 10.1097/MCA.0000000000000107

[13] Buja LM, Entman ML. Modes of myocardial cell injury and cell death in ischemic heart disease. Circulation. 1998; **98**:1355-1357. DOI: 10.1161/01.CIR.98.14.1355

[14] Chaikovsky I, Auth-Eisernitz S, Avolin B, et al. Atlas of typical magnetocardiographic maps for diagnosis of CAD within ST-T interval. In: Proc. of 14th International Conference on Biomagnetism, Boston. 2004. pp. 393-394

[15] Primin M, Nedayvoda I. Mathematical model and measurement algorithms for a dipole source location. International Journal of Applied Electromagnetics and Mechanics. 1997; **8**(2):119-131

[16] Primin M, Nedayvoda I. Inverse problem solution algorithms in magnetocardiography: New analytical approach and some results. International Journal of Applied Electromagnetics and Mechanics. 2009;**29**(2):65-81. DOI: 10.3233/JAE-2009-1001

[17] Primin MA, Nedayvoda IV. A method and an algorithm to reconstruct the spatial structure of current density vectors in magnetocardiography. Cybernetics and Systems Analysis. 2017; **53**(3):485-494. DOI: 10.1007/s10559-017-9950-6

[18] Primin M, Chaikovsky I, Berndt C, Nedayvoda I. Layer-to-layer heart electrical image based on magnetocardiography data in comparison with perfusion image based on PET. International Journal of Bioelectromagnetic. 2003;**5**(1):27-28

[19] Cerqueira MD, Weissman NJ, Dilsizian V, Jacobs AK, Kaul SLaskey WK›Pennell DJ. Standardized myocardial segmentation and nomenclature for tomographic imaging of the heart. A statement for Healthcare Professionals from the Cardiac Imaging Committee of the Council on Clinical Cardiology of the American Heart Association. Circulation. 2002;105(4): 539–542. DOI: 10.1067/mnc.2002.123122

[20] Chaikovsky I, Primin M, Nedayvoda I, Mjasnikov G, Kazmirchyk A, Lutay M, et al. Monitoring of myocardial viability in patients with myocardial infarction based on magnetocardiographic analysis of ventricular depolarisation. Journal of the American College of Cardiology. 2018;**72**(16):C89. DOI: 10.1016/j.jacc.2018.08.475

[21] Callard F, Perego E. How and why patients made Long Covid. Society Science Medicine. 2021;**268**:113426

[22] Metkus TS, Sokoll LJ, Barth AS, Czarny MJ, Hays AG, Lowenstein CJ, et al. Myocardial injury in severe COVID-19 compared with non-COVID-19 acute respiratory distress syndrome. Circulation. 2021;**143**:553-565. DOI: 10.1161/CIRCULATIONAHA.120.050543

[23] Puntmann VO, Carerj ML, Wieters I, et al. Outcomes of cardiovascular magnetic resonance imaging in patients recently recovered from coronavirus disease 2019 (COVID-19). JAMA Cardiology. 2020;**5**(11):1265-1273. DOI: 10.1001/jamacardio.2020.3557

[24] Bossuyt PM, Irwig L, Craig J, Glasziou P. Comparative accuracy: Asse ssing new tests against existing diag nostic pathways. British Medical Journal. 2006;**332**(7549):1089-1092